

# Interactive learning environment for diagnostic radiography with real-time X-ray simulation and patient positioning

Aaron Sujar<sup>a,b,\*</sup>, Marcos García<sup>a</sup>, Luis Pastor<sup>a</sup>, Graham Kelly<sup>c,b</sup>, Franck P.Vidal<sup>b</sup>

<sup>a</sup>*Grupo de Modelado y Realidad Virtual, Universidad Rey Juan Carlos, Spain*

<sup>b</sup>*Bangor University, United Kingdom*

<sup>c</sup>*Shrewsbury and Telford Hospital NHS Trust*

---

## Abstract

We present an interactive learning environment for diagnostic radiography. Our aim is to provide a validated software that can be used to teach radiography using real-time interactive X-ray simulation. Patient positioning can be performed by rotating any joint of the virtual patient. The tool can be used within a lecture to illustrate cases of interest, show specific errors, the effect of the X-ray machine parameters, etc. that would have been difficult (if not impossible) to encounter during the training due to the harmful nature of ionising radiations.

We adapted a fast and accurate character animation technique so that the user can import any kind of anatomic models, move the joints of the virtual patient into the required position, and deform the skin surface and the internal soft tissues accordingly. gVirtualXRay, an open source library to simulate X-rays, is used to generate the corresponding radiographs in realtime. Parameters of the X-ray machine, e.g. beam collimation, beam spectrum, etc. can also be changed by the user and the effect of the changes can be visualised without delay.

A face and content validation study has been conducted. 18 participants were recruited to evaluate our software using a questionnaire. The results show that our tool is realistic in many ways (72% of the participants agreed that the simulations are visually realistic), useful (67%) and suitable (78%) for teaching X-ray radiography.

It is a vital aspect of undergraduate training that mistakes are learnt from to ensure they are not replicated within the real clinical setting. However, trainees are not allowed any mistake in patients due to the use of ionising radiations. Our interactive learning environment for diagnostic radiography enables educators to bridge the disconnects between theory and practice by using a virtual X-ray room within the classroom without using real patients and avoiding any kind of radiation risk.

**Keywords:** Real-time simulation, interactive simulation, character animation, interactive learning environment, X-rays, diagnostic radiography

---

\*Corresponding author.

Email address: [aaron.sujar@urjc.es](mailto:aaron.sujar@urjc.es) (Aaron Sujar)

1      **1. Introduction**

2      Projectional radiography (also called projection radiography, and X-ray radiography) is a very common medical imaging tool that supports clinicians in the diagnostic  
3      of certain diseases, infections, injuries (e.g. bone fractures), and to locate foreign objects. It can be used in almost every part of the patient's body although each specific  
4      body location requires a given patient position and X-ray machine set up, in particular  
5      collimation of the X-ray source, voltage of the X-ray tube, time of exposure, distance  
6      source to patient, and distance source to detector or film.

7      Undergraduate radiographer training within the UK is a mix of academic theory and  
8      clinical practice. Trainee radiographers learn theoretical information such as anatomy  
9      and radiation physics. Theoretical information is learnt within the classroom setting  
10     however, many institutions utilise creative simulations in order for the trainee to ex-  
11     perience the clinical environment within a non-clinical setting such as the university.  
12     Depending on the university facilities trainees also x-ray phantom anatomy in order to  
13     further their understanding of radiation physics principles without the risk of biologi-  
14     cal damage to living tissue. Trainees can then see the effect of imaging principles such  
15     as exposure factors in real time, a practice that could not be performed on living tis-  
16     sue. Teaching cases are utilised within the academic setting again to demonstrate clin-  
17     ical cases. They are compilations of patient histories including their medical images,  
18     recorded discussions, notes and annotations. Trainees can then study well-document  
19     cases through large image datasets. University hospitals and medical schools often  
20     build their own repositories. However, there are now more and more online public re-  
21     sources where radiographers can access vast sets of images from any part of the human  
22     anatomy [1].

23     Nowadays, digital technologies are more ubiquitous than ever and smartphones  
24     start to play a big role in learning. Some institutions have created mobile phone apps  
25     in which trainees can look up images, fill in questionnaires, e.g. [UBC Radiology](#) [2].  
26     This type of resources are playing an increasing role in the curriculum of trainees in  
27     radiology and diagnostic radiography. Nevertheless, all these images show the final  
28     results and do not describe the whole procedure. Also, as there are static images, it  
29     is not possible to modify any acquisition parameter (e.g. tube voltage) to interactively  
30     visualise the changes in the X-ray radiographs corresponding to this parameter modifi-  
31     cation. According to the old adage, "we learn from our mistakes". However, trainees  
32     are not allowed any mistake in patients due to the use of ionising radiations. For safety  
33     reasons, projections obtained with different set ups never come from the same patient,  
34     hindering any possible comparison. Furthermore, patient positioning is a key step and  
35     it cannot be easily learned from the final images.

36     It is a vital aspect of undergraduate training that mistakes are learnt from to ensure  
37     they are not replicated within the real clinical setting. For trainees to further under-  
38     stand errors, an X-ray room is required within the academic setting. The use of an  
39     anatomical phantom is also then required to X-ray in order to demonstrate these errors.  
40     This cannot be easily conducted within a typical classroom setting and therefore con-  
41     stitutes a separate teaching session. This could lead to a disconnect between theory and  
42     practice.

43     Virtual reality (VR) medical simulation is playing an increasing role in the physi-

46 cians' curriculum, such as surgeons and other specialists [3, 4]. They are applied to  
47 a wide variety of medical procedures [5, 6]. Such applications are used for safe and  
48 effective training purposes. Unlike traditional methods (using cadavers, animals or  
49 mannequins), computerised simulators permit new physicians to improve and develop  
50 their non-cognitive skills in a cheap and safe environment [7]. It is also possible to use  
51 such simulators without the close supervision of an expert.

52 Recent advances in computer graphics (CG) allow the development of new simula-  
53 tors that can be used in the apprenticeship of radiographers. In this context, it is worth  
54 to mention two computerised simulators. On one hand, [8] is a simulator for training in  
55 interventional radiology where fluoroscopy (real-time X-ray images) is used to guide  
56 a needle towards an anatomical structure. Despite of the fact that the simulator has  
57 an interactive X-ray simulation and the deformation of lung tissues, there is only one  
58 example of patient and it is only focused on the chest area.

59 On the other hand, ProjectionVR™ is a simulator that immerses the user into a re-  
60 alistic 3D X-ray room to simulate the complete procedure [9]. With virtual digitised  
61 patient data, it replicates an interactive learning environment without the risk of radi-  
62 ation exposure to students or patients. Although it provides a variety of real cases, the  
63 greatest limitation of this tool is that users always load the same static images with the  
64 same examples and they cannot produce new X-ray images instantly. There are only  
65 pre-computed images and users are not able to re-position a particular patient or play  
66 with anatomy variations and pathologies. Another simulator, called medspace.VR,  
67 provides an immersive 3D environment [10]. Although it allows to modify the patient  
68 position, only skin and bones seem to be present in the produced X-ray images and  
69 there is a lack of variety in the anatomic models.

70 Patient variability is desirable so that trainees can be exposed to all kind of possibil-  
71 ities, e.g. from underweight to overweight patients, from babies to elderly patients. It  
72 is also beneficial for simulators to emulate specific scenarios (e.g. a detecting foreign  
73 bodies, or collapsed lung) which would have been difficult to routinely encounter as a  
74 student.

75 In this paper, we propose an X-ray projectional radiograph simulator that can be  
76 used as an interactive teaching and learning environment where teachers and students  
77 are able to review numerous virtual patients with the possibility to manipulate the pa-  
78 tient positioning and the X-ray machine parameters in realtime. Our tool was designed  
79 with the following requirements in mind:

- 80     • It could use a wide variety of existing virtual patient models.
- 81     • Users can interactively manipulate the virtual patient to the position required in  
82       any given procedure.
- 83     • Users can observe the X-ray image immediately as they change the virtual pa-  
84       tient's position, X-ray source's position or any other X-ray machine parameter.

85 To fulfil the requirements mentioned above, our simulator is made of three main  
86 modules: the Virtual X-ray Imaging Library (gVirtualXRay), the Virtual Patient Posi-  
87 tioning System (VPPS) and the courseware. The first one is in charge of generating  
88 the X-ray image from a triangular mesh in realtime. This module is able to simulate

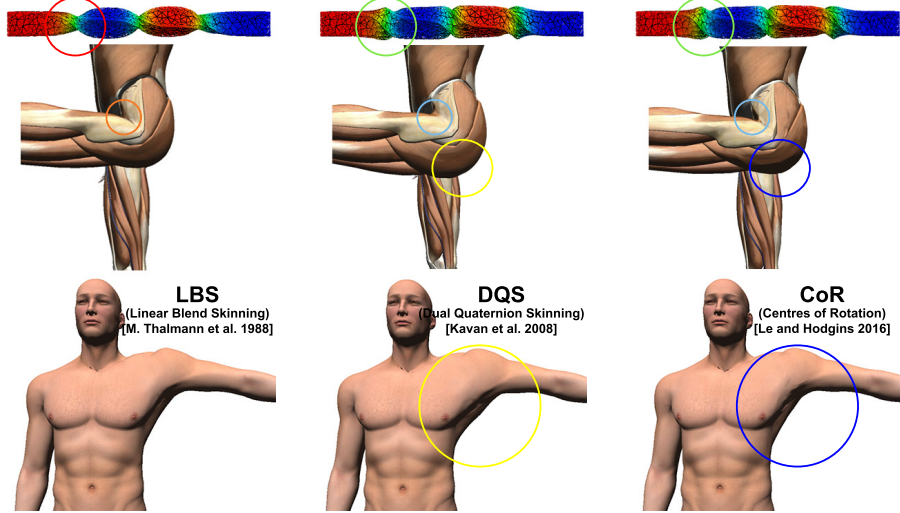
89 the most relevant X-ray configuration parameters. VPPS transforms the anatomy of a  
90 virtual patient to the desired position. It was designed to be flexible to deal with as  
91 many virtual patients as possible. With this goal in mind, our algorithm works with  
92 incomplete anatomical models (skin and bones are the minimum tissues required) and  
93 the biomechanical properties of the virtual patient tissues are not required. Finally,  
94 both modules are integrated in a courseware environment, which implements the user  
95 interface and characterises the most important steps in X-ray projectional radiography.

96 Section 2 details the work related to our application. It focuses on character ani-  
97 mation and X-ray simulation. Section 3 discusses the technical choices made: Using  
98 a real-time animation of the anatomy and a real-time framework for the simulation of  
99 X-ray images. The main features of our X-ray radiograph simulator are reviewed in  
100 Section 4. Section 5 shows the final results achieved in this project. It reviews three  
101 use cases (teacher's use, student's use, and exercises). A face and content validation  
102 study is also provided (see Section 6). Section 7 provides our conclusions and discuss  
103 possible future work. Finally, the appendix describes a YouTube Playlist with videos  
104 that illustrate the most important functionalities of our interactive teaching and learning  
105 environment.

106 **2. Related work**

107 To provide the most true-to-life experience and offer a broad variety of cases, com-  
108 puterised medical simulators aim to be as realistic as possible. For this purpose, virtual  
109 human models are required [11]. There are commercially available anatomical virtual  
110 human models, such as *ZygoteBody™* [12]. An alternative is the use of real patient  
111 data captured using medical imaging techniques such as computed tomography (CT),  
112 magnetic resonance imaging (MRI) and/or ultrasound (US). The rational is to provide  
113 more realistic models as there are directly derived from actual patient data [13]. Al-  
114 though the new generation of medical simulators have recently begun to use specific  
115 patient data [14], the main problem is that those virtual patients are usually given in  
116 a specific subject position. Also, the patient's position in the medical scanner may be  
117 different from the one required by the simulator. Some particular procedures need the  
118 patient model in a different position than it was initially recorded. The consequence is  
119 that the patient data is very static and limited, and it does not represent the majority of  
120 clinical cases. Character animation from CG (i.e. techniques from the film and video  
121 game industries) can be used to move bones and update the skin surface accordingly.  
122 However, medical simulators still need a method that deals with anatomy animation  
123 including deformation of internal soft-tissues.

124 To animate virtual patient models as realistically as possible, we have considered  
125 bio-mechanical and musculoskeletal techniques and physically-based models from the  
126 CG literature. We can found some examples where the muscle behaviour is simulated  
127 efficiently [15]. For most of these techniques, a user must perform some steps manually  
128 and, in general, bio-mechanical models are not complete and localised only on a part of  
129 the human anatomy [16]. Others physically-based techniques try to preserve muscle's  
130 volume [17]. Muscle tissues present other problems as it is usually required to retrieve  
131 the muscle's image in relaxed and extended positions. Also, there are techniques that  
132 retrieve muscle-skeletal models from medical images [18].



(a) LBS is the classic technique but suffers from candy-wrapper artefact.

(b) DQS solves candy-wrapper artefact but deformed tissues may change in volume.

(c) COR is more robust to the candy wrapper and joint-bulging artefacts [23].

Figure 1: Differences between the LBS, DQS and COR skinning techniques. The red circle depicts a candy-wrapper artefact; the orange circle depicts a collapsing elbow and the yellow circles show joint-bulging artefacts. Green circles are used when candy-wrapper artefacts are solved; cyan circles when the collapsing elbow artefact is solved and blue circles when joint-bulging artefacts are solved.

133 All these techniques do not run at interactive rates and may require detailed information  
 134 of the patient which is not readily available. Often, not all patient tissues are  
 135 captured properly or the tissue’s mechanical properties are not easy to extract from the  
 136 medical images. Furthermore, simulators need other anatomical structures aside from  
 137 simulating muscles and skeleton.

138 On the contrary, geometrically-based algorithms usually run in real-time and they  
 139 usually produce plausible results. Skeletal animation is the most used 3D CG technique  
 140 to animate articulated characters. The most widely used technique is Linear Blending  
 141 Skinning (LBS) [19], but it suffers well-known artefacts such as collapsing elbows  
 142 or candy wrapper effect which do not help to get realism in a simulator. Another  
 143 technique commonly used is Dual Quaternion Skinning (DQS) [20], it solves LBS’s  
 144 problems but occasionally introduces joint-bulging artefact where meshes increase in  
 145 volume. Numerous alternatives to LBS and DQS can be found in the literature [21]  
 146 to address some of the deficiencies mentioned above, but at the cost of decreasing  
 147 the computational performance or leading to other artefacts. In [22], Le and Hodgin  
 148 solve those artefacts without needing more computational power but a high number of  
 149 centres of rotation must be initially calculated (see Figure 1).

150 To ease the deployment of new models by users with no or limited knowledge in  
 151 CG, we have focused on methods that can provide virtual patient data automatically.  
 152 Baran and Popović [24] proposed an automatic algorithm where they adapt a virtual

153 skeleton to any 3D model. More recent work improves this method to deal with point  
154 handles, virtual bones and cages [25] (a cage defines an enclosure, using a 2D polygon  
155 or a 3D polyhedron, which is used to control the deformation of an arbitrary topology).  
156 It is also possible to use registration to transfer data from MRI to a desired anatomical  
157 model [26]. This technique is, however, not focused on animation and does not run  
158 interactively. As an alternative, Sújar *et al* proposed a relatively similar method to de-  
159 form the anatomical structures [23]. Furthermore, it is an automatic method to animate  
160 human character's anatomy in realtime.

161 Another component that is required to build this interactive learning environment  
162 is the X-ray image simulator. Both accuracy and speed are requirements. Physically-  
163 based simulation frameworks exist. They are often aimed at particle physics and/or  
164 medical physics research and focus on accuracy rather than speed. These frameworks  
165 usually rely on Monte Carlo (MC) methods because they produce very realistic im-  
166 ages [27, 28, 29]. Particles, here photons, are generated. The path of each photon  
167 through matter is tracked. At each step of the simulation, random events, such as  
168 scattering and absorption, may occur depending on probability laws that rely on the  
169 photon's energy and the properties of the material crossed by the photon. However,  
170 MC methods are not applicable to real-time interactive applications because they have  
171 to calculate probabilistic X-ray interaction models for the transport of photons in mat-  
172 ter and it is time consuming: To generate a relatively noise-free image, days or weeks  
173 of calculation may be needed. As a fast alternative, deterministic calculation based on  
174 ray-tracing is often used to solve the Beer-Lambert law [30, 31, 32, 33]. Freud *et al* pro-  
175 posed an alternative model for deterministic simulation [34]. It relies on the traditional  
176 graphics pipeline by using a modified Z-buffer algorithm [35, 36] called L-buffer. It  
177 has been ported to the graphics processing unit (GPU) using OpenGL and its OpenGL  
178 Shading Language (GLSL) [37]. It shares the same technologies used by modern video  
179 games to provide a real-time X-ray image simulation tool. It is now available as an  
180 Open Source project, gVirtualXRay (<http://gvirtualxray.sourceforge.net/>),  
181 and can be used with various programming language such as Python, R, Ruby, GNU  
182 Octave, etc. [38]. Other GPU implementations have also been reported [39].

### 183 3. Simulator Components

184 We propose a tool that allows teachers and students to interact with the X-ray con-  
185 figuration and the patient's positioning without any kind of radiological risk to the  
186 patient or even the radiographer. Our approach relies on two computationally intensive  
187 components: i) a real-time character animation framework (VPPS) that allows the  
188 virtual patient to change positions, with his/her internal anatomy being deformed ac-  
189 cordingly, and ii) an X-ray simulation library (gVirtualXRay) that generates physically-  
190 based radiographic images in realtime. Besides, the courseware module integrates both  
191 components, providing a graphical interface and simulator training functions.

192 The VPPS precomputes a significant amount of data to achieve interactive frame  
193 rates. Fortunately, all these computations can be performed only once per model. One  
194 of the most challenging requirements we face in our research was to simplify the in-  
195 corporation of new virtual patient models. Therefore, the VPPS component is split in  
196 two modules. The first one computes required pre-process data for each module and

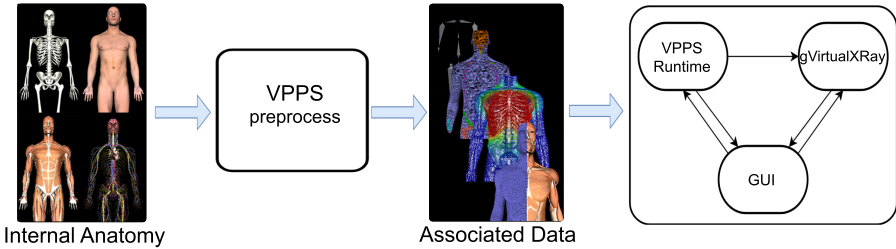


Figure 2: Simulator architecture: i) anatomical structures are preprocessed once per character, ii) then the X-Ray simulator loads the patient anatomic and the precomputed data and finally the courseware drives the training session controlling the VPPS module and gVirtualXRay. This architecture allows to run the simulation at interactive rates.

197 the second one adapts the patient positioning on users demand. Figure 2 summarises  
198 the overall architecture of our software.

### 199 *3.1. Virtual Patient Positioning System*

200 To let the user select a position interactively, we adapt the internal and external  
201 anatomical models of a virtual character to any desired position. We decided to follow  
202 a purely geometrical approach based on an improved skeletal animation technique [23],  
203 instead of a fully physically-based simulation algorithm, in order to meet the following  
204 requirements:

- 205 • It has to be flexible to incorporate as many existing 3D patient models as possi-  
206 ble.
- 207 • It has to minimize the user intervention when adding new virtual patients.
- 208 • It has to run in realtime.

209 Skeletal animation is commonly used in the computer graphics industry to animate  
210 articulated 3D models. This type of techniques transfers the movement of a virtual  
211 skeleton to a boundary representation (B-rep) of a virtual character. The procedure is  
212 divided into three stages: rigging, weighting and skinning. The virtual skeleton, which  
213 is a hierarchical set of virtual bones, is created in the rigging phase. The weighting  
214 phase computes the influence of each virtual bone on the model vertices. Finally, the  
215 bones' movements are transferred to the vertices through a skinning technique. The  
216 main limitation of this traditional workflow is that the rigging and weighing steps are  
217 usually performed manually by a 3D artist to provide a plausible animation. Although  
218 there exist several approaches to automatise these two steps [40, 41], they are designed  
219 to work with B-reps and they cannot be used to deform internal soft-tissues.

220 Our method relies on a fully automatic procedure that transfers the bone move-  
221 ments to all tissue models. In contrast to classical skeletal animation techniques, our  
222 animation pipeline applies the bones movements to a Lagrangian mesh that discretise  
223 the interior of the virtual patient. We use the volumetric Lagrangian mesh to interpolate  
224 a displacement field, which is used to deform any available internal or external patient

225 anatomy. In order to build the virtual skeleton and the volumetric Lagrangian mesh,  
226 the meshes corresponding to bones and the skin have to be correctly labelled and they  
227 are the only required tissues (i.e. internal tissues are optional). We have divided the  
228 animation workflow in 5 stages:

- 229 1. Rigging: We adapt a predefined virtual skeleton to the labelled bone tissue.
- 230 2. Volumetrisation: This stage automatically builds a volumetric Lagrangian mesh.
- 231 3. Weighting: Our method estimates the influence of the virtual bones on the volu-  
232 metric mesh vertices, using the diffusion equation for the stationary case.
- 233 4. Mapping: Aiming at accelerating the real-time animation of the patient anatomy,  
234 all the virtual tissues are mapped into the volumetric mesh.
- 235 5. Skinning: The virtual bones movements are applied to the volumetric mesh and  
236 then transferred to the patient tissues.

237 The first four steps are computationally expensive and they have to be executed  
238 only once per patient. Therefore, we have grouped them in a VPPS Preprocess Module.  
239 Besides the skinning phase it can be implemented to run in modern GPUs and achieve  
240 interactive frame rates, even for complex models (see Section 5).

### 241 3.2. Virtual X-ray Imaging Library

242 A deterministic simulation tool is required to generate images in realtime. Monte  
243 Carlo simulation is not suitable as it cannot provide real-time performance. gVirtualXRay  
244 has been selected for the X-ray generation as it is an open-source library that  
245 makes use of portable technologies, such as the C++ language, OpenGL and GLSL for  
246 the core library, and Simplified Wrapper and Interface Generator (SWIG) to generate  
247 binders to other programming languages (to-date C#, Java, Octave, Perl, Python 2 and  
248 Python 3, R, and Ruby are supported) [42]. gVirtualXRay also makes use of triangular  
249 meshes to describe the patient’s anatomy. This requirement is shared with the real-time  
250 patient positioning component. This is the most common data representation in real-  
251 time 3-D graphics. Digitally reconstructed radiograph (DRR), a well-known technique  
252 to generate radiographs from CT scans, has been discarded for this reason [43]. It is  
253 not convenient to implement a character animation model with CT data. Also, GPU  
254 handles on the triangular meshes are actually shared between the two components gVirtualXRay  
255 and the real-time patient positioning component to increase performance.

256 gVirtualXRay implements Freud *et al*’s L-buffer principle [34] on the GPU. It relies  
257 on a modified rendering pipeline from 3-D computer graphics. The L-buffer aims at  
258 computing the path length of X-rays through polygon meshes, from the X-ray source  
259 to every pixel of the detector. It is then used to solve the Beer-Lambert law (also called  
260 attenuation law) from polygon meshes. It was first implemented on GPU with a mono-  
261 chromatic beam spectrum (all the photons have the same energy) and for parallel pro-  
262 jections (e.g. to mimic a source far away from the scanned object as with a synchrotron)  
263 and infinitesimally small point sources [37]. Extra rendering passes (i.e. loops in the  
264 algorithm) were added to the rendering pipeline to allow the use of polychromatic  
265 beam spectra and to model the focal spot of an X-ray tube [44]. The current version  
266 of gVirtualXRay relies on the XCOM Photon Cross Sections Database from the Na-  
267 tional Institute of Standards and Technology (NIST) to compute the mass attenuation

268 coefficient of the material of the scanned objects [45]. The material can be defined as  
 269 a chemical element (e.g. hydrogen), a mixture (e.g. “Ti90Al1V4” for a titanium alloy  
 270 with small amounts of aluminium, 6%, and vanadium, 4%), a compound (e.g. “H<sub>2</sub>O”  
 271 for water), or a Hounsfield unit. We chose the latter as it is commonly understood in the  
 272 medical community. Hounsfield units are then converted into their respective chemical  
 273 compositions and densities [46]. A quantitative validation study has been conducted  
 274 to assess the accuracy of the simulated X-ray images [38]. Geant4, a state-of-the-art  
 275 Monte Carlo radiation transport code by the European Organization for Nuclear Re-  
 276 search (CERN), is used to generate some X-ray radiographs. Each image required  
 277 about two weeks of computations on HPC Wales’ supercomputer. Similar radiographs  
 278 are simulated on the GPU with gVirtualXRay in milliseconds. Corresponding images  
 279 are then compared (see Figure 3 for an example). Test images produced with gVirtu-  
 280 alXRay are perfectly correlated with the ground-truth images produced using Geant4.

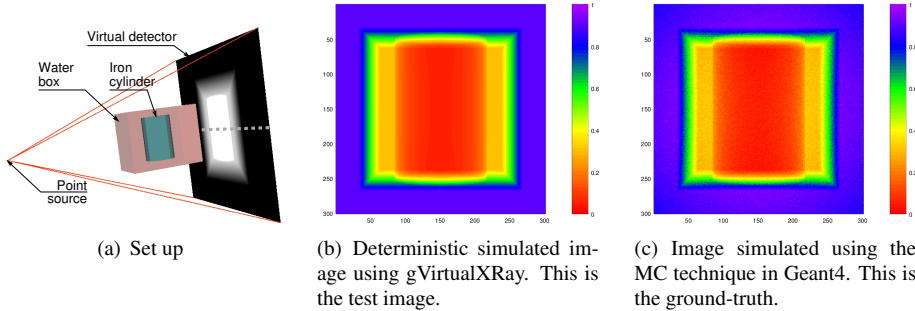


Figure 3: Example of validation test using a simple test case.

#### 281 4. Courseware

282 The courseware is in charge of developing the training capabilities of the simulator,  
 283 integrating the previously described modules and providing a graphical user interface  
 284 (GUI). Figure 4 shows how the GUI looks like and the main functionalities of the  
 285 simulator. All the GUI widgets related to the position functionality are grouped in the  
 286 upper left corner of the window. In the lower left corner, the X-ray machine setup can  
 287 be configured. The list of patient tissues is located in the upper right corner. Finally, in  
 288 the lower right corner, the corresponding X-ray image is shown and it can be modified  
 289 using the mouse.

290 This section describes its most important features. First, we explain how the pro-  
 291 cedure is characterised and then, the lecturing and self guided-training functionalities  
 292 are described.

##### 293 4.1. Simulation of the X-Ray procedure

###### 294 4.1.1. Positioning the patient

295 In projectional radiography, the positioning of a patient is essential in order to get  
 296 the best image whilst reducing the radiation dose to the minimum requirement. As



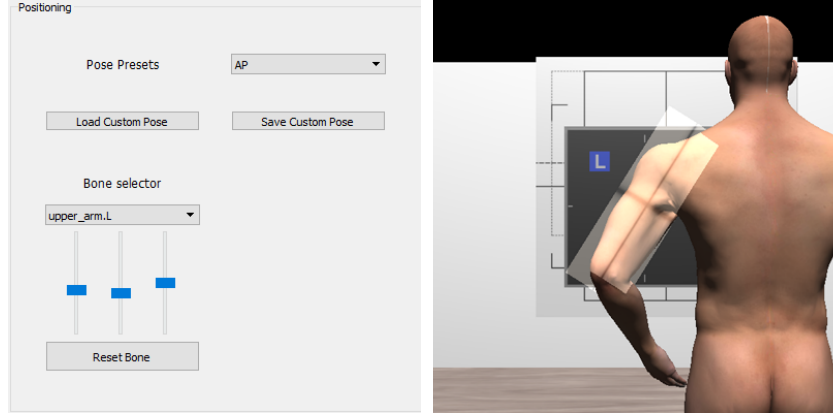
Figure 4: GUI of our projectional radiography simulator: (a) patient positioning options, (b) centring, tube voltage, source-object distance and source-cassette distance configuration (c) collimation setup, (d) tissue visibility and material properties, (e) side marker's selection and digital image manipulation.

described in the radiographer curriculum [47], the users can choose if the patient is standing up or lying down. Note that the VPPS makes use of a purely geometrical algorithm and does not take into account the effect of gravity. Then, users are able to define the position of a particular body part through the GUI, using a variety of methods : (i) Common positions used in radiography are preset and they can be chosen from a top-down list; (ii) They can eventually choose any body part and move it directly. The users can then modify the position of any bone by altering the rotation angles of the corresponding joints using sliders; (iii) They can estimate the position of virtual patient using motion capture with an off-the-shelf peripheral such as the Microsoft Kinect (see <https://youtu.be/1s-eTT1pCy8> for evidence). In Figure 5, the upper arm was moved to get an lateral humerus projection. Any position can be saved so that teachers can make pre-recorded positions available to students or for future use in the classroom. Depending on the lecturer demands any of the previously described techniques can be removed from the GUI. <https://youtu.be/zitw5-Xk4dY> is a link to a video that illustrates patient positioning.

#### 4.1.2. X-ray setup

Three components need to be set to simulate an X-ray image. The properties of the X-ray source, the X-ray detector (or cassette) and a virtual anatomy need to be known:

- The *X-ray source* is defined by its position, shape (e.g. parallel beam, point source, or focal spot) and beam spectrum (monochromatic or polychromatic).
- The *X-ray detector* is defined by its position, size, resolution and orientation.
- *Each anatomical structure* is defined by its surface as a triangular mesh and its material properties so that its linear attenuation coefficients can be computed to



(a) A user defines the left arm position via the (b) Corresponding 3D visualisation where the  
GUI. virtual patient's left arm has been moved accord-  
ingly.

Figure 5: An example of virtual patient positioning.

320 solve the Beer-Lambert law. We rely here on Hounsfield values and convert them  
321 into mass attenuation coefficients and densities [46].

322 Other parameters may also be included, e.g. collimation (see below).

323 In this medical application, whenever possible we favour parameters that are mean-  
324 ingful for the targeted community of users rather than parameters required by the sim-  
325 ulator. The user can control the relative distance between the X-ray source and the  
326 detector or cassette (known as *source to image distance (SID)* in radiography) and the  
327 distance between the X-ray source and the patient (known as *source to object distance  
(SOD)*). *Centring point* is another technical term used in radiography. Centring is the  
328 focus point of the primary X-ray beam in relation to anatomy. This point is dictated by  
329 the anatomy that is trying to be demonstrated within an X-ray image. This point will  
330 represent the middle of the resultant X-ray.

331 Centring and positioning of the patient are heavily correlated, and they actually  
332 define the relative positions of the X-ray source, of the cassette and of the patient.  
333 Therefore appropriate centring and positioning are necessary to maintain the radiation  
334 dose to its strict necessary minimum. It is assumed that a radiographer will always  
335 ensure that the centre of the body part lies at the middle of the cassette.

336 “Collimation” is another common technical term used in radiography. Lead plates  
337 or leaves can be placed at the front of the X-ray tube to limit the exposure to ionising  
338 radiation to a given area of the body. As lead is a material that heavily attenuates  
339 X-rays, hardly any radiation is deposited in the tissues protected by the collimator.  
340 Therefore appropriate collimation is also important to ensure the area of interest is  
341 definitely included on the image, limit the radiation field to that area of interest, reduce  
342 scatter in order to maintain the image quality and limit the radiation exposure of organs  
343 at risk.

Such important aspects of X-ray radiography can be reproduced in our virtual environment. The X-ray source and cassette move as the user move the mouse in 3D visualisation window. The user can also use the GUI buttons to finely tune the position into a correct centring (see Figure 7). The X-ray beam is represented by the light projection on the patient' skin and cassette (see Figure 6) as it is the case in the X-ray room (see Figure 15(a)).

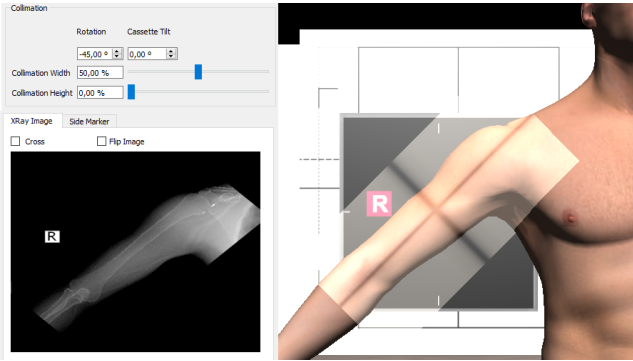


Figure 6: Collimation configuration to target the X-ray beam on the humerus only. It is rotated by 45° and the height of the beam has been reduced.

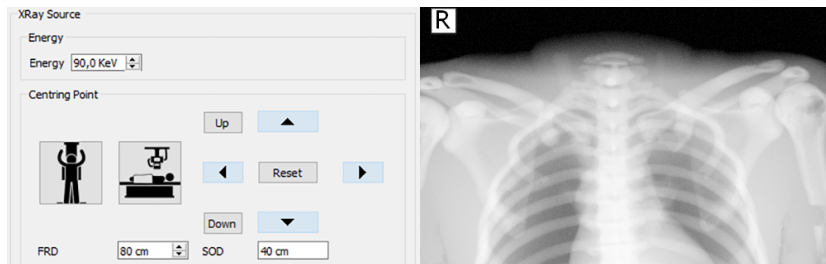
The X-ray beam spectrum corresponds to a tabulated list of number of photons and corresponding photon energies in kiloelectron volt (keV). In a clinical environment this is controlled by radiographers via the peak kilovoltage (kVp) of the current applied to the X-ray tube. Exposure factors play an important role in X-ray projectional diagnosis because they can affect the quality of the produced radiograph. An inappropriate exposure may decrease the contrast in X-ray images. In order to avoid mistakes and avoid taking the same radiograph several times, trainees must understand how radiation is produced by an X-ray tube and what/how parameters affect the image quality. An X-ray tube contains a cathode to produce electrons and an anode, i.e. a target on which the electrons will collide. If the electrons has a sufficient energy, X-rays will be created. The operator can control the electrical parameters (voltage applied to the tube in kilovolt (kV) and current intensity in milliampere-second (mAs)) and exposure time in fraction of a second. The voltage controls the energy of the X-ray photons produced by the tube. mAs controls the amount of photons produced over a set amount of time (seconds). For medical diagnosis in radiography, the anode is usually made of tungsten. Voltages in the 55-125 kV range are commonly used in clinical routine. Corresponding spectra can be simulated using the tungsten anode spectral model using interpolating polynomials (TASMIP) algorithm [48]. For each voltage in the range 30-140 kV, it produces a list of photon energies in keV and relative number of photons. The user can select the voltage in kV, and the corresponding beam spectrum is used to in the simulation by gVirtualXRay.

Changing the kV value will produce different X-ray images. The X-ray radiation is absorbed differently by soft than dense structures. The level of absorption varies with the photon energy, but not linearly. When the kV increases, the X-ray photons can

375 penetrate more without being absorbed. On the one hand, if the kV value is too low,  
 376 the image will be whiter and more blurred. On the other hand, if the kV value is too  
 377 high, the image will be over-exposed and too dark. Our simulator can replicate such  
 behaviour (see Figure 7).



(a) X-ray image simulated using a 60 kVp X-ray tube voltage. The incident energy produced by the X-ray tube is too low to sufficiently penetrate the tissues and differentiate them on the X-ray image.



(b) X-ray image simulated using 90 kVp X-ray tube voltage. The contrast between tissues has improved.

Figure 7: Effect of the X-ray tube voltage on an X-ray image of the chest.

378 Note that due to the deterministic nature of the X-ray simulation algorithm, mAs  
 379 cannot be directly taken into account. However it is possible to mimic a low mAs value  
 380 by adding Poisson noise to the simulated X-ray image.  
 381

#### 382 4.1.3. *Cassette's side markers*

383 In clinical radiography, an anatomical marker is placed within the field of the X-  
 384 ray source, and clear of the area of interest. It aims to identify the left- and right-hand  
 385 sides of the patient. This is because the left-hand side of the patient may not be on  
 386 the left of the image. This practice is mandatory to avoid misinterpretation of the  
 387 X-ray image. In our tool, a 2D widget allows to interactively place a side marker  
 388 over the cassette using the mouse. This 2D widget transfers this 2D position on the  
 389 cassette to the 3D visualisation of the cassette in the virtual environment. Additionally,  
 390 this side marker appears on the X-ray image and can be saved in an image file. See  
 391 <https://youtu.be/EDJM3pSWtgo> for an illustrative video. Figure 8 shows the side  
 392 markers in the 3D visualisation and in the corresponding X-ray image.

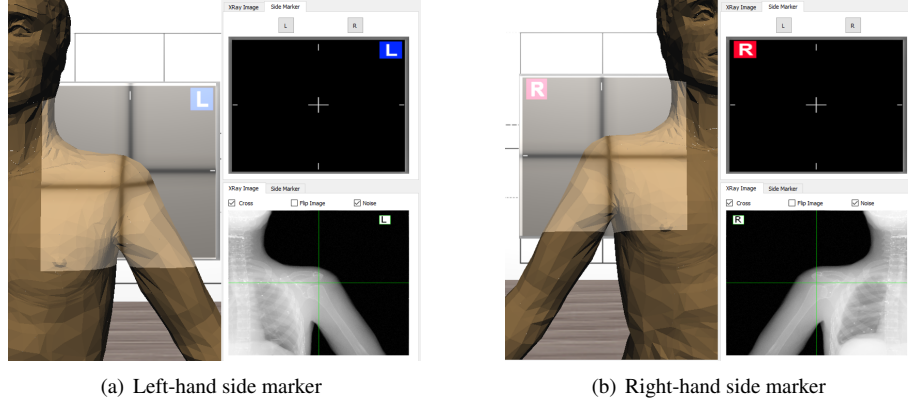


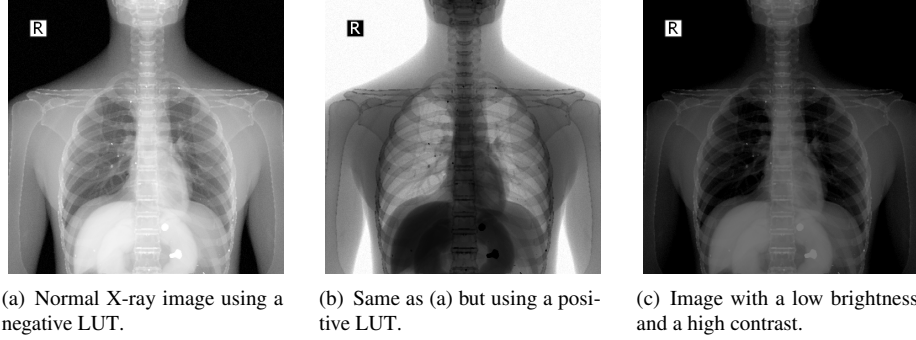
Figure 8: The user can select between the left and right side markers and place it over the cassette.

#### 393 4.1.4. Digital image manipulation

394 Nowadays, digital X-ray detectors are used in modern hospitals rather than traditional X-ray film. The X-ray image is captured directly to a bitmap by the detector, and  
 395 it is possible to display it using a computer. The greatest advantage of digital imaging  
 396 is the ability to duplicate, store and manipulate the data. For example, image filter-  
 397 ing can be used to reduce minor problems due to overexposure or underexposure, and  
 398 perform some measurements (e.g. compute the distance between two different anatomical  
 399 landmarks). Digital images can also be used in computer-aided diagnostic (CAD)  
 400 software. Our user interface provides a few simple image processing filters that allow  
 401 users to enhance resulting images (e.g. to get a better interpretation of the anatomical  
 402 tissues). A Log-Scale filter and a Gamma filter can be selected to improve the final  
 403 image. The brightness and contrast can also be altered to emphasise each tissue or  
 404 highlight a particular zone. In medical applications, X-ray images are often shown in  
 405 *negative*, so that bones are in white and air in black. All these filters can be easily used  
 406 by clicking with the mouse over the X-ray image. Figure 9 shows examples of image  
 407 manipulation applied on the same X-ray image. In Figure 9(a), coins can easily be seen  
 408 on the image compared to Figures 9(b) and 9(c). Also, the anatomical side marker is  
 409 present to determine the anatomical side of body on the radiographic image. Finally,  
 410 users can save any X-ray radiograph they want to in an image file on the hard drive.  
 411 See <https://youtu.be/x7KGsNSMSh8> for a video that focuses on the digital image  
 412 manipulation.  
 413

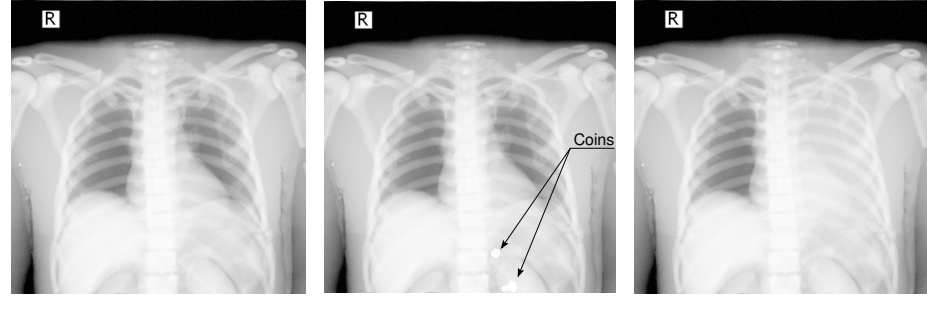
#### 414 4.2. Lecturing features

415 Our simulator provides additional features which will support the instructor in the  
 416 classroom environment, although they are not directly related to the simulation of any  
 417 step of the diagnostic radiography procedure. The system allows to show and hide  
 418 specific tissues of the virtual patient at run time. For example, the user can modify the  
 419 opacity of the skin surface to reveal internal structures in the 3D visualisation. This



(a) Normal X-ray image using a negative LUT.  
 (b) Same as (a) but using a positive LUT.  
 (c) Image with a low brightness and a high contrast.

Figure 9: Our tool allows digital image manipulation.



(a) Normal AP Chest X-ray image.  
 (b) Same image as (a) but with foreign objects in the stomach.  
 (c) Same image as (a) but with a collapsed lung.

Figure 10: The X-Ray attenuation properties of the tissues can be modified to simulate different scenarios.

420 way students can understand the relationship between the different body tissues and  
 421 X-ray images.

422 It is also possible to modify the tissues properties with respect to X-ray attenuation  
 423 using the Hounsfield Scale. Hounsfield values can be converted into list of chemical  
 424 elements, etc. [46] so that corresponding linear attenuation coefficients can be com-  
 425 puted from photon cross-sections [45] to solve the Beer-Lambert law for any incident  
 426 energy. Being able to change the tissues properties allows teachers to show a variety  
 427 of diseases, e.g. a calcified bone, a collapsed lung (see Figure 10(c)), or an air-filled  
 428 stomach. It is even possible to introduce foreign objects inside the internal anatomy.  
 429 For example, Figures 9 and 10(b) show coins in the stomach. See the following video  
 430 for further details: <https://youtu.be/02K2ojcExTc>.

#### 431 4.3. Self-guided training

432 Performing diagnostic radiography requires both theoretical and non-cognitive skills.  
 433 The only effective way of acquiring non-cognitive skills is practice. It is now well es-  
 434 tablished that VR resources and computerised simulators can be exploited to guide and

435 boost the trainees' learning process. Interactive tools can also be designed to promote  
436 self-directed learning. With this regard, our simulator provides a guided mode that  
437 leads users along the procedure. This mode explains the X-ray projection procedure  
438 step-by-step and offers additional information if the user requires it. Finally, the system  
439 evaluates the user's performance and retrieves assessment metrics. Besides, we offer set  
440 of non-guided exercises that allows the instructor to check the evolution of the trainees.  
441 Finally, we have created a set of videos to help the users to get used to the simulator.  
442 See the following videos for further information: <https://youtu.be/EdyDqvGr8ww>  
443 and <https://youtu.be/WFOAVSLXufs>.

444 **5. Results**

445 The proposed X-Ray simulator offers a teaching and learning platform where third  
446 party anatomic models can be easily integrated. To test the viability of our approach,  
447 we incorporated the following models:

- 448 • ZygoteBody™ 3D Poly Models [12]. This set of virtual patient models provide  
449 B-Reps of the most important tissues. We used female (ZF) and male (ZM)  
450 models.
- 451 • Anatomium™ 3D Human Anatomy Digital Data Sets [49] offer several virtual  
452 patients. Similarly to ZygoteBody, they include the B-reps of several tissues.  
453 We used one of the available male models.
- 454 • Voxel-Man's Segmented Inner Organs [50, 51]. This model is composed by a  
455 set of segmented volumetric images obtained from the Visible Human data set.  
456 To incorporate this model, we generate surface meshes using the marching cubes  
457 algorithm [52].

458 Figure 11 depicts the visual results obtained for these models and Table 1 shows the  
459 complexity of each model. As it was expected, the quality of the final image depends  
460 to a large extend on the quality of the virtual patient model. We found that some gen-  
461 eral purpose models need further preprocessing to obtain plausible images. Bones are  
462 made of two types of tissues. The outer layer of bones is called cortical bones. They are  
463 strong and dense. The inner layer, called trabecular bone, is a lot less dense. Comercial  
464 3D virtual models often only provide the bone structures as the surface of the cortical  
465 bones. Trabecular bone are almost systematically ignored. Other types of tissues are  
466 also provided as their superficial representation, i.e. without nothing inside. However,  
467 gVirtualXRay works as a ray tracer where a ray goes through an anatomical structure  
468 (front face of a triangle) and get out of the same structure (back face of a triangle) in or-  
469 der to calculate the light attenuation depending on the material properties associated to  
470 this anatomical structure and the length of ray crossing it. This solution does not work  
471 particularly well with bones because their internal layers attenuate X-rays a lot less.  
472 As a consequence, if no particular care is given to bones, they will have an homoge-  
473 neous look in the simulated X-ray images, which is not very realistic (see Figure 12(a)).  
474 To solve this deficiency, we added a new mesh for each bone to depict the trabecular  
475 bones. It can be efficiently achieved by duplicating the surface mesh of the cortical

Table 1: Model complexity.

<b>Model</b>	Superficial Mesh		Volumetric Mesh	
	<b>Vertices</b>	<b>Triangles</b>	<b>Nodes</b>	<b>Tetrahedrons</b>
<u>ZygoteBody</u> <sup>TM</sup> Male [53]	1317862	2601469	553412	2576779
<u>ZygoteBody</u> <sup>TM</sup> Female [53]	1468989	2896011	492646	2314456
<u>Anatomium</u> Male [49]	790461	1570778	767325	3411170
<u>Segmented Inner Organs</u> [51]	591265	1184325	242033	1182485

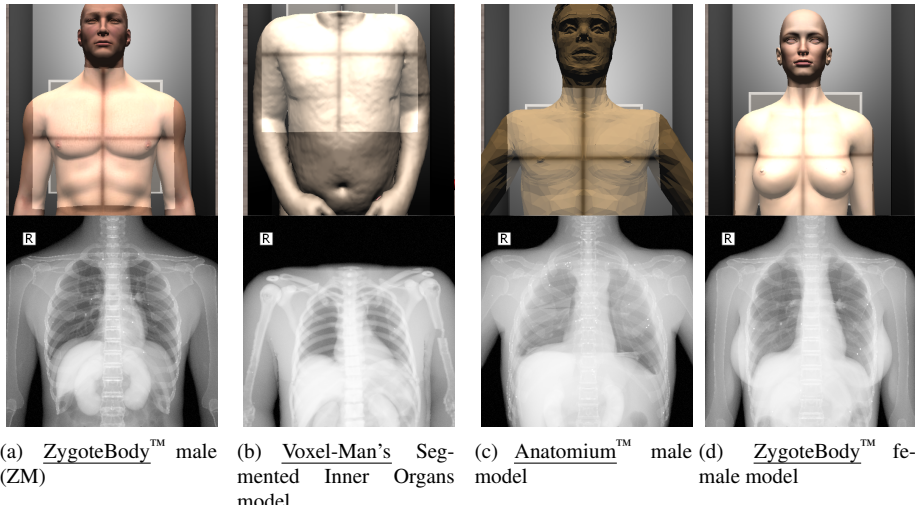
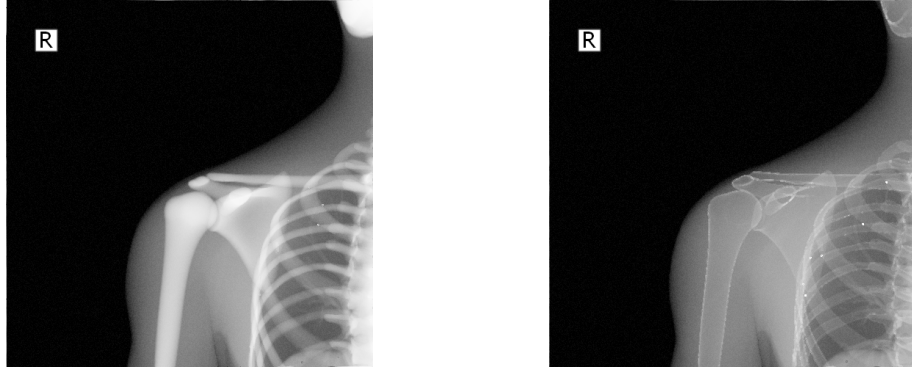


Figure 11: Results obtained using different anatomical models.

476 bones, shrinking them a little bit, and inverting their normal vectors. Figure 12 depicts  
 477 the difference between the original meshes without trabecular bones and the modified  
 478 meshes with trabecular bones. Note that this issue does not occur when working with  
 479 surface meshes extracted from segmented CT dataset as cortical and trabecular bones  
 480 are easy to identify and separate in CT data. Regarding the patient positioning, the  
 481 VPPS module worked seamlessly with all the models used in the evaluation.

482 VR simulators required interactive frame rates to guaranty an adequate user experience.  
 483 For this reason, VPPS and gVirtualXRay were implemented to run efficiently  
 484 in modern GPUs. Besides, both modules share GPU memory to reduce the data transferred  
 485 through the system busses. The performance was tested on an Intel®i7-3770 @  
 486 3.7GHz CPU with 16GB of Random Access Memory (RAM) and a NVIDIA® Quadro  
 487 K5000 graphics card with 4GB of graphics memory. In the worse case (ZM), the frame  
 488 rate is over 30 fps. However, the preprocessing module requires about 7 minutes for



(a) Original ZygoteBody™ model without soft and hard bone differentiation.

(b) Same model as (a) but with added internal structures.

Figure 12: Solving the absence of internal structures in bone.

489 each virtual patient.

#### 490 **6. Face and content validation**

491 A combined face and content validation study has been conducted to gather feed-  
 492 back from experts. The face validation evaluates the level of resemblance between  
 493 the simulation and the procedure performed in the real world. The content validation  
 494 quantifies what the tool actually teaches/trains (e.g. psycho-motor skills or anatomy).  
 495 It ascertains that the simulation correctly replicate the steps and features of the real  
 496 procedure. Face and content validation is often performed using questionnaires. Our  
 497 questionnaire include questions designed i) to characterise the cohort of participants to  
 498 assess their level of expertise in X-ray radiography, ii) for the face validation, and iii)  
 499 for the content validation. The questionnaire is available at <https://goo.gl/forms/cghkCHtylUt8ixzw1>.

500 18 participants were recruited. The average number of years of experience is  
 501 12.5 years, the standard deviation is 11.74 years: This cohort is well experienced to  
 502 assess our tool. There are 9 males and 9 females. It allows us to check if there is any  
 503 gender effect. All the participants but one are qualified. Although most participants  
 504 were from the United Kingdom (15 of them), 1 participant was from Canada, 1 from  
 505 France, and 1 from Spain.

506 16 participants exercise their art in radiography, 1 participant is a medical doctor  
 507 (MD) in stomatology and another one in nuclear medicine. Due to his speciality, the  
 508 stomatologist reported be confident when taking X-ray radiographs. However, the MD  
 509 in nuclear medicine did not. Both MDs reported being extremely confident when in-  
 510 terpreting X-ray radiographs. As a consequence, their answers were relevant to our  
 511 study.

512 14 statements related to the realism of the simulator and its functionalities were  
 513 used for the face validity (see Table 2). Figure 13 shows the corresponding results

for all participants. The percentage of ‘strongly agree’ or ‘agree’ answers for each

Face validity
F1: The patient model before selecting the posing is visually realistic.
F2: The deformation of the patient’s internal anatomy is visually realistic.
F3: The previously described steps characterize the procedure in a realistic way.
F4: The placement of the side markers on the x-ray image is visually realistic.
F5: The changes in the final x-ray image due to the adjustment of the beam direction and FRD are visually realistic.
F6: The adjustment of the centre is visually realistic.
F7: The changes in the final x-ray image due to the collimation adjustment are visually realistic.
F8: The changes in the final x-ray image due to beam energy configuration are visually realistic.
F9: In general, the changes in the final x-ray image due to modification of the different parameters are visually realistic.
F10: The adjustment of the brightness and contrast settings is visually realistic.
F11: The use of image filters is visually realistic.
F12: The simulation of diseases is visually realistic.
F13: The inclusion of foreign objects in the virtual patient is visually realistic.
F14: Generally speaking, the simulator is visually realistic.

Table 2: Face validity statements

515 statement is above 50%. Between 70% and 79% of the participants ‘strongly agree’ or  
 516 ‘agree’ with seven of the statements (F3, F4, F5, F6, F7, F9, and F14). It is between  
 517 60% and 69% for five statements (F1, F2, F8, F10, and F11). It is between 50% and  
 518 59% for only two statements (F12 and F13), which are related to the mimicking of  
 519 disease and the inclusion of foreign objects. These functionalities were implemented  
 520 using a naive approach (e.g. changing the HU value for the collapsed lung). The overall  
 521 feedback is positive (F14). We can conclude that this initial face validation is promising  
 522 as it clearly shows that most participants ‘strongly agree’ or ‘agree’ that our simulation  
 523 tool is realistic in many ways.

524  
 525 For content validity, 11 statements related to the main purpose of the simulator and  
 526 the courseware were included in the content validity (see Table 3). Figure 14 shows the  
 527 corresponding results for all participants. A pattern similar to the face validation is  
 528 observed for the content validation. Between 70% and 79% of the participants ‘strongly  
 529 agree’ or ‘agree’ with six of the statements (C1, C2, C4, C7, C10, and C11). It is  
 530 between 60% and 69% for four of the statements (C3, C5, C6, and C8). It is 50% for  
 531 C9. Again, the overall feedback is positive. Participants judged that the tool is useful  
 532 as a teaching tool for X-ray radiography (C8), but less as a self-guided training tool  
 533 (C9). However, the results show the suitability of our tool as a teaching tool (C10) and  
 534 as a self-guided training tool (C11).

535 Participants also had the opportunity to provide free comments. Such comments  
 536 were very positive:

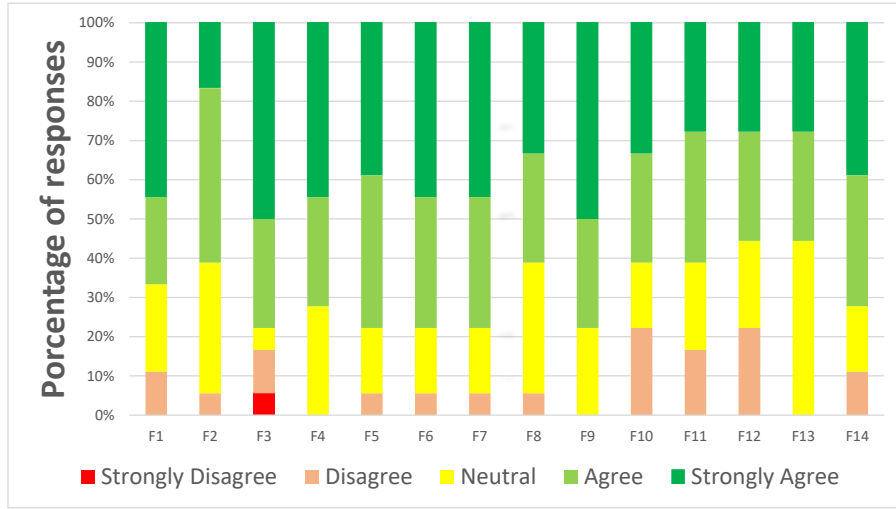


Figure 13: Result of the face validation study using a Likert scale.

537 “I think this would be a really excellent tool for student to learn from  
 538 and improve their skills for when they go in placement.”

539 and

540 “Great idea”

## 541 7. Conclusions

542 In this paper, we presented a VR teaching and learning environment for diagnostic  
 543 radiography. It relies on i) an interactive character animation method for the patient  
 544 positioning and deformation of internal tissues, and ii) a real-time X-ray simulation  
 545 library. We developed a courseware module that turns our tool into a training sys-  
 546 tem. It is now well established that VR resources and computerised simulators can  
 547 be exploited to guide and boost the trainees’ learning process. Radiographers have to  
 548 know both how to position a patient and how to tune an X-ray tube to avoid clinically  
 549 unnecessary radiation doses and repetitive acquisitions of X-ray images. Our system  
 550 provides a safe environment where the procedure can be rehearsed, reducing all kinds  
 551 of radiological risk to the patient or even the radiographer. It is important to highlight  
 552 that the proposed system does not substitute traditional teaching methods but enhance  
 553 the learning process overcoming their main limitations. Figure 15 compares a specific  
 554 projection from a text book [47] with a simulation of the same projection. The real  
 555 and the virtual patient used to generate both images are also shown. Both, real patient  
 556 databases and text books are the preferred approaches to get theoretical skills, while  
 557 our simulator allows to interactively perform the main steps of the procedure in order  
 558 to train non-cognitive skills.

559 We have designed the courseware module to include functionalities to assist the  
560 teacher during the lecture and for self-directed learning. Allowing repetitions without  
561 any radiation risk, it is useful in both environments. Since, the positioning tool and the  
562 X-ray image simulation achieve interactive frame rates, the teachers and students can  
563 select the anatomy position and the machine set-up and see the corresponding changes  
564 in X-ray image in realtime. In the classroom, teachers can discuss a given procedure,  
565 e.g. what is important and the pitfalls to avoid. They can interactively show a good  
566 picture (good positioning, centring, collimation, and setting of the X-ray machine) and  
567 bad ones. In contrast, the courseware guides the students through the procedure and  
568 they can see the actual consequences of their mistakes. Additionally, we provide a  
569 non-guided mode, where the system asks the student for a specific projection (see  
570 Figure 16)

571 Our solution was designed to facilitate the incorporation of new virtual patient mod-  
572 els. Section 5 shows how several third party models were successfully integrated. This  
573 functionality was particularly challenging since our tool allows the user to modify in-  
574 teractively the patient's position and very few constraints are imposed to the models.  
575 Indeed, only the skin and bone tissues of the virtual patient need to be properly la-  
576 belled. Currently, the scientific community is putting a lot of effort in developing new  
577 techniques for creating virtual patient to be used in VR medical trainers and plan-  
578 ners [54, 55]. The proposed X-Ray simulator will benefit from these interest as most  
579 of these techniques are compatible with our approach. On the same way, other medical  
580 imaging process can be simulated and integrated in the same tool. Recently, there are  
581 projects trying to simulate effectively techniques like MRI or CT which requires some  
582 patient position knowledge.

583 The positioning system sacrifices accuracy in favour of computational performance  
584 and flexibility. Natural phenomena such as gravity cannot be simulated. As a result  
585 of using a geometrically-based algorithm, its plausible positions are only oriented for  
586 training and educational purposes.

587 We have also conducted a set of experiments to probe the face and content validity  
588 of our tool. The overall results of the face validity show that our tool is realistic in  
589 many ways. However, the simulation of specific diseases and the inclusion of foreign  
590 objects need to be improved. The overall results of the content validity show both the  
591 usefulness and suitability of our tool in teaching and/or learning X-ray radiography.  
592 However, further tests would be needed to perform a construct validation study, i.e. to  
593 assess the actual benefit of using of our tool in teaching.

594 Nevertheless, this tool has some limitations about the full procedure. There are  
595 important concerns like the patient preparation which is not covered in this tool:

- 596 • Physician must employ appropriate and effective communication with patients
- 597 • Patient is indicated about remove clothes or artefacts over the relevant examina-  
598 tion area.
- 599 • Recommendations about use lead rubber either on patients or radiographers.
- 600 • Some assessments which involve medical conditions or protocols like pregnancy,  
601 correct patient identification, etc.

602 This is because the tool is intended as a teaching tool by an educator/lecturer rather  
603 than a self-guided training tool by students.

604 Finally, we would like to remark that computerised systems are very good registering  
605 the user actions. All this information can be used to develop a set of assessment  
606 metric that will serve to provide the trainees with information to boost their self-  
607 learning processes and to evaluate their proficiency. The definition of a valid set of  
608 assessment metrics will be explored in our future work.

609 **Acknowledgements**

610 The research leading to these results has been partially funding by the following  
611 entities: the Spanish Government [Cajal Blue Brain Project, Spanish partner  
612 of the Blue Brain Project initiative from EPFL; and grants TIN2014-57481-C2-1-R,  
613 TIN2017-83132-C2-1-R and FPU15/05747] and European Commission [under grant  
614 agreements: HBP - Human Brain Project - FET Flagship HBP604102; RaSimAS: Re-  
615 gional Anaesthesia Simulator and Assistant - FP7-ICT 610425, and Fly4PET: Fly Al-  
616 gorithm in PET Reconstruction for Radiotherapy Treatment Planning - FP7-PEOPLE-  
617 2012-CIG 321968].

618 Some examples were based on the Visible Human male data set (National Library  
619 of Medicine) and the Segmented Inner Organs (Voxel-Man).

620 We would like to thanks HPC Wales for the use of its supercomputer during the  
621 validation of gVirtualXRay and NVIDIA for donating the GPU that was used during  
622 the implementation of gVirtualXRay.

623 **Acronyms**

624 **B-rep** boundary representation.

625 **CAD** computer-aided diagnostic.

626 **CERN** European Organization for Nuclear Research.

627 **CG** computer graphics.

628 **COR** Centre of Rotation.

629 **CT** computed tomography.

630 **DQS** Dual Quaternion Skinning.

631 **DRR** digitally reconstructed radiograph.

632 **GLSL** OpenGL Shading Language.

633 **GPU** graphics processing unit.

634 **GUI** graphical user interface.

- 635   **keV** kiloelectron volt.
- 636   **kV** kilovolt.
- 637   **kVp** peak kilovoltage.
- 638   **LBS** Linear Blending Skinning.
- 639   **LUT** lookup table.
- 640   **mAs** milliampere-second.
- 641   **MC** Monte Carlo.
- 642   **MD** medical doctor.
- 643   **MRI** magnetic resonance imaging.
- 644   **NIST** National Institute of Standards and Technology.
- 645   **RAM** Random Access Memory.
- 646   **SID** source to image distance.
- 647   **SOD** source to object distance.
- 648   **SWIG** Simplified Wrapper and Interface Generator.
- 649   **TASMIP** tungsten anode spectral model using interpolating polynomials.
- 650   **US** ultrasound.
- 651   **VPPS** Virtual Patient Positioning System.
- 652   **VR** Virtual reality.

653   **References**

- 654   [1] P. Deshpande, A. Rasin, E. Brown, J. Furst, D. Raicu, S. Montner, S. Armato III,  
655       An integrated database and smart search tool for medical knowledge extraction  
656       from radiology teaching files, in: Proceedings of Workshop on Medical Informat-  
657       ics and Healthcare, 2017, pp. 10–18.
- 658   [2] R. Spouge, Review of UBC Radiology Teaching App, Journal of Digital Imag-  
659       ing [doi:10.1007/s10278-017-0034-y](https://doi.org/10.1007/s10278-017-0034-y).
- 660   [3] A. Bernardo, Virtual reality and simulation in neurosurgical training, World Neu-  
661       rosurgery 106 (2017) 1015–1029. [doi:10.1016/j.wneu.2017.06.140](https://doi.org/10.1016/j.wneu.2017.06.140).

- 662 [4] G. S. Ruthenbeck, K. J. Reynolds, Virtual reality for medical training: the state-  
663 of-the-art, *Journal of Simulation* 9 (1) (2015) 16–26. [doi:10.1057/jos.2014.14](https://doi.org/10.1057/jos.2014.14).
- 665 [5] J. Cecil, A. Gupta, M. Pirela-Cruz, An advanced simulator for orthopedic surgical  
666 training, *International journal of computer assisted radiology and surgery* 13 (2)  
667 (2018) 305–319. [doi:10.1007/s11548-017-1688-0](https://doi.org/10.1007/s11548-017-1688-0).
- 668 [6] P. Korzeniowski, R. J. White, F. Bello, VCSim3: a VR simulator for cardiovascular  
669 interventions, *International journal of computer assisted radiology and surgery* 13 (1)  
670 (2018) 135–149. [doi:10.1007/s11548-017-1679-1](https://doi.org/10.1007/s11548-017-1679-1).
- 671 [7] R. Patel, R. Dennick, Simulation based teaching in interventional radiology train-  
672 ing: is it effective?, *Clinical Radiology* 72 (3) (2017) 266.e7–266.e14. [doi:  
673 10.1016/j.crad.2016.10.014](https://doi.org/10.1016/j.crad.2016.10.014).
- 674 [8] P.-F. Villard, F. P. Vidal, L. Ap Cenydd, R. Holbrey, S. Pisharody, S. Johnson,  
675 A. Bulpitt, N. W. John, F. Bello, D. Gould, Interventional radiology virtual sim-  
676 ulator for liver biopsy, *International journal of computer assisted radiology and*  
677 *surgery* 9 (2) (2014) 255–267. [doi:10.1007/s11548-013-0929-0](https://doi.org/10.1007/s11548-013-0929-0).
- 678 [9] M. Shanahan, Student perspective on using a virtual radiography simulation, *Radi-  
679 graphy* 22 (3) (2016) 217–222. [doi:10.1016/j.radi.2016.02.004](https://doi.org/10.1016/j.radi.2016.02.004).
- 680 [10] P. Bridge, T. Gunn, L. Kastanis, D. Pack, P. Rowntree, D. Starkey, G. Mahoney,  
681 C. Berry, V. Braithwaite, K. Wilson-Stewart, The development and evaluation of  
682 a medical imaging training immersive environment, *Journal of Medical Radiation  
683 Sciences* 61 (3) (2014) 159–165. [doi:10.1002/jmrs.60](https://doi.org/10.1002/jmrs.60).
- 684 [11] B. Preim, P. Saalfeld, A survey of virtual human anatomy education systems,  
685 *Computers & Graphics* 71 (2018) 132–153. [doi:10.1016/j.cag.2018.01.  
686 005](https://doi.org/10.1016/j.cag.2018.01.005).
- 687 [12] Zygote Media Group, ZygoteBody, <https://www.zygotebody.com/>, ac-  
688 cessed: 2018-11-08 (2018).
- 689 [13] J. E. de Oliveira, P. Giessler, A. Keszei, A. Herrler, T. M. Deserno, Surface mesh  
690 to voxel data registration for patient-specific anatomical modeling, in: *Medical  
691 Imaging 2016: Image-Guided Procedures, Robotic Interventions, and Modeling*,  
692 Vol. 9786, International Society for Optics and Photonics, 2016, p. 978625. [doi:  
693 10.1117/12.2217491](https://doi.org/10.1117/12.2217491).
- 694 [14] J. Zhang, J. Chang, X. Yang, J. J. Zhang, Virtual reality surgery simulation: A  
695 survey on patient specific solution, in: J. Chang, J. J. Zhang, N. Magnenat Thal-  
696 mann, S.-M. Hu, R. Tong, W. Wang (Eds.), *Next Generation Computer Anima-  
697 tion Techniques*, Vol. 10582 of *Lecture Notes in Computer Science*, Springer Inter-  
698 national Publishing, Cham, 2017, pp. 220–233. [doi:10.1007/978-3-319-  
699 69487-0\\\_16](https://doi.org/10.1007/978-3-319-69487-0\_16).

- 700 [15] A. Rajagopal, C. L. Dembia, M. S. DeMers, D. D. Delp, J. L. Hicks, S. L. Delp,  
 701 Full-body musculoskeletal model for muscle-driven simulation of human gait,  
 702 IEEE Transactions on Biomedical Engineering 63 (10) (2016) 2068–2079. [doi:10.1109/TBME.2016.2586891](https://doi.org/10.1109/TBME.2016.2586891).
- 704 [16] A.-E. Ichim, P. Kadlecak, L. Kavan, M. Pauly, Phace: Physics-based face mod-  
 705 eling and animation, ACM Trans. Graph. 36 (4) (2017) 153:1–153:14. [doi:10.1145/3072959.3073664](https://doi.org/10.1145/3072959.3073664).
- 707 [17] Y. Fan, J. Litven, D. K. Pai, Active volumetric musculoskeletal systems, ACM  
 708 Trans. Graph. 33 (4) (2014) 152:1–152:9. [doi:10.1145/2601097.2601215](https://doi.org/10.1145/2601097.2601215).
- 709 [18] T. T. Dao, P. Pouletaut, F. Charleux, Á. Lazáry, P. Eltes, P. P. Varga, M. C. H. B.  
 710 Tho, Multimodal medical imaging (CT and dynamic MRI) data and computer-  
 711 graphics multi-physical model for the estimation of patient specific lumbar spine  
 712 muscle forces, Data & Knowledge Engineering 96-97 (2015) 3–18. [doi:10.1016/j.datak.2015.04.001](https://doi.org/10.1016/j.datak.2015.04.001).
- 714 [19] N. Magnenat-Thalmann, R. Laperrière, D. Thalmann, Joint-dependent local de-  
 715 formations for hand animation and object grasping, in: Proceedings on Graphics  
 716 Interface '88, Canadian Information Processing Society, Toronto, Ont., Canada,  
 717 Canada, 1988, pp. 26–33.  
 718 URL <http://dl.acm.org/citation.cfm?id=102313.102317>
- 719 [20] L. Kavan, S. Collins, J. Žára, C. O'Sullivan, Skinning with dual quaternions, in:  
 720 Proceedings of the 2007 Symposium on Interactive 3D Graphics and Games, I3D  
 721 '07, ACM, New York, NY, USA, 2007, pp. 39–46. [doi:10.1145/1230100.1230107](https://doi.org/10.1145/1230100.1230107).
- 723 [21] N. A. Rumman, M. Fratarcangeli, State of the art in skinning techniques for ar-  
 724 ticulated deformable characters, in: Proceedings of the 11th Joint Conference  
 725 on Computer Vision, Imaging and Computer Graphics Theory and Applications:  
 726 Volume 1: GRAPP, SCITEPRESS-Science and Technology Publications, Lda,  
 727 2016, pp. 200–212.
- 728 [22] B. H. Le, J. K. Hodgins, Real-time skeletal skinning with optimized centers of ro-  
 729 tation, ACM Trans. Graph. 35 (4) (2016) 37:1–37:10. [doi:10.1145/2897824.2925959](https://doi.org/10.1145/2897824.2925959).
- 731 [23] A. Sújar, J. J. Casafranca, A. Serrurier, M. García, Real-time animation of human  
 732 characters' anatomy, Computers & Graphics 74 (2018) 268–277. [doi:10.1016/j.cag.2018.05.025](https://doi.org/10.1016/j.cag.2018.05.025).
- 734 [24] I. Baran, J. Popović, Automatic rigging and animation of 3D characters, ACM  
 735 Trans. Graph. 26 (3) (2007) 72:1–72:8. [doi:10.1145/1276377.1276467](https://doi.org/10.1145/1276377.1276467).
- 736 [25] A. Jacobson, I. Baran, J. Popović, O. Sorkine-Hornung, Bounded biharmonic  
 737 weights for real-time deformation, Commun. ACM 57 (4) (2014) 99–106. [doi:10.1145/2578850](https://doi.org/10.1145/2578850).

- 739 [26] A.-H. Dicko, T. Liu, B. Gilles, L. Kavan, F. Faure, O. Palombi, M.-P. Cani,  
 740 Anatomy transfer, *ACM Trans. Graph.* 32 (6) (2013) 188:1–188:8. [doi:10.1145/2508363.2508415](#).
- 742 [27] S. Agostinelli, et al., Geant4—a simulation toolkit, *Nucl Instrum Methods Phys  
 743 Res A* 506 (3) (2003) 250–303. [doi:10.1016/S0168-9002\(03\)01368-8](#).
- 744 [28] A. Bielajew, et al., History, overview and recent improvements of EGS4,  
 745 Tech. rep., Stanford Linear Accelerator Center (SLAC) (2004). [doi:10.2172/839781](#).
- 747 [29] J. Baró, J. Sempau, J. M. Fernández-Varea, F. Salvat, PENELOPE: An algorithm  
 748 for Monte Carlo simulation of the penetration and energy loss of electrons and  
 749 positrons in matter, *Nucl Instrum Methods Phys Res B* 100 (1) (1995) 31–46.  
 750 [doi:10.1016/0168-583X\(95\)00349-5](#).
- 751 [30] F. Inanc, J. N. Gray, T. Jensen, J. Xu, Human body radiography simulations: de-  
 752 velopment of a virtual radiography environment, in: Proc.SPIE, Vol. 3336, 1998,  
 753 p. 8. [doi:10.1117/12.317091](#).
- 754 [31] A. Glière, Sindbad: From CAD model to synthetic radiographs, in: Review of  
 755 Progress in Quantitative Nondestructive Evaluation: Volume 17A, Springer US,  
 756 Boston, MA, 1998, pp. 387–394. [doi:10.1007/978-1-4615-5339-7\\_49](#).
- 757 [32] G.-R. Tillack, C. Bellon, C. Nockemann, Computer simulation of radiographic  
 758 process - a study of complex component and defect geometry, in: Review of  
 759 Progress in Quantitative Nondestructive Evaluation: Volume 14, Springer US,  
 760 Boston, MA, 1995, pp. 665–672. [doi:10.1007/978-1-4615-1987-4\\_82](#).
- 761 [33] D. Lazos, Z. Kolisti, N. Pallikarakis, A software data generator for radio-  
 762 graphic imaging investigations, *IEEE Transactions on Information Technology  
 763 in Biomedicine* 4 (1) (2000) 76–79. [doi:10.1109/4233.826863](#).
- 764 [34] N. Freud, P. Duvauchelle, J. M. Létang, D. Babot, Fast and robust ray casting  
 765 algorithms for virtual X-ray imaging, *Nucl Instrum Methods Phys Res B* 248 (1)  
 766 (2006) 175–180. [doi:10.1016/j.nimb.2006.03.009](#).
- 767 [35] W. Straßer, Schnelle kurven- und flächendarstellung auf graphischen sichtgeräten,  
 768 Ph.D. thesis, TU Berlin (1974).
- 769 [36] E. E. Catmull, A subdivision algorithm for computer display of curved surfaces,  
 770 Ph.D. thesis, The University of Utah (1974).
- 771 [37] F. P. Vidal, M. Garnier, N. Freud, J. M. Létang, N. W. John, Simulation of X-ray  
 772 Attenuation on the GPU, in: W. Tang, J. Collomosse (Eds.), *Theory and Practice  
 773 of Computer Graphics*, The Eurographics Association, 2009, pp. 25–32. [doi:  
 774 10.2312/LocalChapterEvents/TPCG/TPCG09/025-032](#).
- 775 [38] F. P. Vidal, P.-F. Villard, Development and validation of real-time simulation of x-  
 776 ray imaging with respiratory motion, *Computerized Medical Imaging and Graph-  
 777 ics* 49 (2016) 1–15. [doi:10.1016/j.compmedimag.2015.12.002](#).

- 778 [39] Q. Gong, R.-I. Stoian, D. S. Coccarelli, J. A. Greenberg, E. Vera, M. E. Gehm,  
 779      Rapid simulation of x-ray transmission imaging for baggage inspection via gpu-  
 780      based ray-tracing, Nuclear Instruments and Methods in Physics Research Section  
 781      B: Beam Interactions with Materials and Atoms 415 (2018) 100–109. [doi:10.1016/j.nimb.2017.09.035](#).
- 783 [40] P. Borosán, M. Jin, D. DeCarlo, Y. Gingold, A. Nealen, RigMesh: Automatic rig-  
 784      ging for part-based shape modeling and deformation, ACM Trans. Graph. 31 (6)  
 785      (2012) 198:1–198:9. [doi:10.1145/2366145.2366217](#).
- 786 [41] C.-H. Huang, E. Boyer, S. Ilic, Robust human body shape and pose tracking, in:  
 787      Proceedings of the 2013 International Conference on 3D Vision, 3DV ’13, IEEE  
 788      Computer Society, Washington, DC, USA, 2013, pp. 287–294. [doi:10.1109/3DV.2013.45](#).
- 790 [42] D. M. Beazley, [SWIG: An easy to use tool for integrating scripting languages with C and C++](#), in: Proceedings of the 4th Conference on USENIX Tcl/Tk Workshop, 1996 - Volume 4, TCLTK’96, USENIX Association, Berkeley, CA, USA, 1996, pp. 15–15.  
 791      URL <http://dl.acm.org/citation.cfm?id=1267498.1267513>
- 795 [43] J. M. Galvin, C. Sims, G. Dominiak, J. S. Cooper, The use of digitally recon-  
 796      structed radiographs for three-dimensional treatment planning and ct-simulation,  
 797      International Journal of Radiation Oncology\*Biology\*Physics 31 (4) (1995)  
 798      935–942. [doi:10.1016/0360-3016\(94\)00503-6](#).
- 799 [44] F. P. Vidal, M. Garnier, N. Freud, J. M. Létang, N. W. John, Accelerated determin-  
 800      istic simulation of x-ray attenuation using graphics hardware, in: Eurographics  
 801      2010 - Poster, Eurographics Association, Norrköping, Sweden, 2010, p. Poster  
 802      5011.
- 803 [45] M. J. Berger, J. H. Hubbell, S. M. Seltzer, J. Chang, J. S. Coursey, R. Sukumar,  
 804      D. S. Zucker, K. Olsen, [XCOM: Photon cross section database](#), Tech. Rep. NB-  
 805      SIR 87-3597, National Institute of Standards and Technology, Gaithersburg, MD  
 806      (2010). [doi:10.18434/T48G6X](#).  
 807      URL <http://physics.nist.gov/xcom>
- 808 [46] W. Schneider, T. Bortfeld, W. Schlegel, Correlation between CT numbers and tis-  
 809      sue parameters needed for Monte Carlo simulations of clinical dose distributions,  
 810      Physics in Medicine & Biology 45 (2) (2000) 459–478. [doi:10.1088/0031-9155/45/2/314](#).
- 812 [47] E. Carver, B. Carver, Medical Imaging: Techniques, Reflection & Evaluation,  
 813      2nd Edition, Elsevier Health Sciences, 2012.
- 814 [48] J. M. Boone, J. A. Seibert, An accurate method for computer-generating tungsten  
 815      anode X-ray spectra from 30 to 140 kV, Medical Physics 24 (11) (1997) 1661–  
 816      1670. [doi:10.1118/1.597953](#).

- 817 [49] 21st Century Solutions Ltd, Digital human 3D body anatomy, <http://www.anatomium.com/>, accessed: 2018-11-08.
- 819 [50] U. Tiede, A. Pommert, B. Pflessner, E. Richter, M. Riemer, T. Schiemann, R. Schubert, U. Schumacher, K. H. Höhne, A high-resolution model of the inner organs based on the visible muman data set, Journal of Visualization 5 (3) (2002) 212–212. [doi:10.1007/BF03182328](https://doi.org/10.1007/BF03182328).
- 823 [51] Segmented Inner Organs (SIO) Group, Voxel-Man, <https://www.voxel-man.com/segmented-inner-organs-of-the-visible-human/>, accessed: 2018-11-08.
- 826 [52] W. E. Lorensen, H. E. Cline, Marching cubes: A high resolution 3D surface construction algorithm, SIGGRAPH Comput. Graph. 21 (4) (1987) 163–169. [doi:10.1145/37402.37422](https://doi.org/10.1145/37402.37422).
- 829 [53] R. Kelc, Zygote body: A new interactive 3-dimensional didactical tool for teaching anatomy, WebmedCentral ANATOMY 3 (1). [doi:10.9754/journal.wmc.2012.002903](https://doi.org/10.9754/journal.wmc.2012.002903).
- 832 [54] W. I. M. Willaert, R. Aggarwal, I. Van Herzele, N. J. Cheshire, F. E. Vermaessen, Recent advancements in medical simulation: patient-specific virtual reality simulation, World journal of surgery 36 (7) (2012) 1703–1712. [doi:10.1007/s00268-012-1489-0](https://doi.org/10.1007/s00268-012-1489-0).
- 836 [55] E. Votta, T. B. Le, M. Stevanella, L. Fusini, E. G. Caiani, A. Redaelli, F. Sotiropoulos, Toward patient-specific simulations of cardiac valves: state-of-the-art and future directions, Journal of biomechanics 46 (2) (2013) 217–228. [doi:10.1016/j.jbiomech.2012.10.026](https://doi.org/10.1016/j.jbiomech.2012.10.026).

840 **Appendix A. YouTube playlist**

841 We provide a YouTube playlist for the reader's convenience. It can  
842 be found at [https://www.youtube.com/playlist?list=PLI54dBkPi2QjkHx10Z6FCmlDW\\_kZUAIX](https://www.youtube.com/playlist?list=PLI54dBkPi2QjkHx10Z6FCmlDW_kZUAIX). It includes the videos as follows:

- 844 • <https://youtu.be/EdyDqvGr8ww> provides an overview of the various steps involved into producing an X-ray image with our tool.
- 846 • <https://youtu.be/zitw5-Xk4dY> illustrates the character animation framework and the real-time deformation of internal soft tissues.
- 848 • <https://youtu.be/1s-eTT1pCy8> provides evidence of motion capture using the Microsoft Kinect to transfer the position of an actual human being to the virtual patient.
- 851 • <https://youtu.be/EDJM3pSWtgo> focuses on the side markers.
- 853 • <https://youtu.be/x7KGsNSMSh8> focuses on digital image manipulation of the produced X-ray image.

- 854     • <https://youtu.be/02K2ojcExTc> shows special cases (collapsed lung and the  
855       insertion of foreign objects).
- 856     • <https://youtu.be/GwWY8AQffEY> shows that our tool can be extended to pro-  
857       vide students with exercises.
- 858     • <https://youtu.be/WFOAVSLXufs> is a longer video, with a summary of the  
859       most important functionalities of our tool.

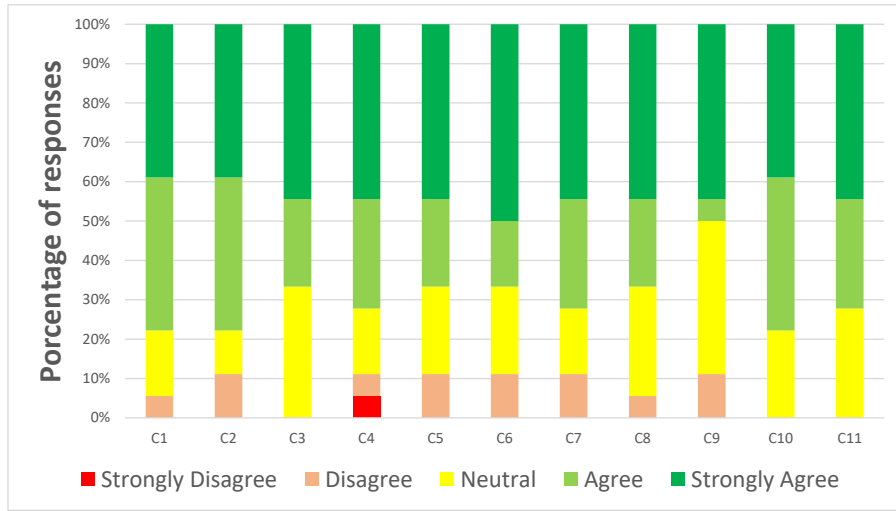


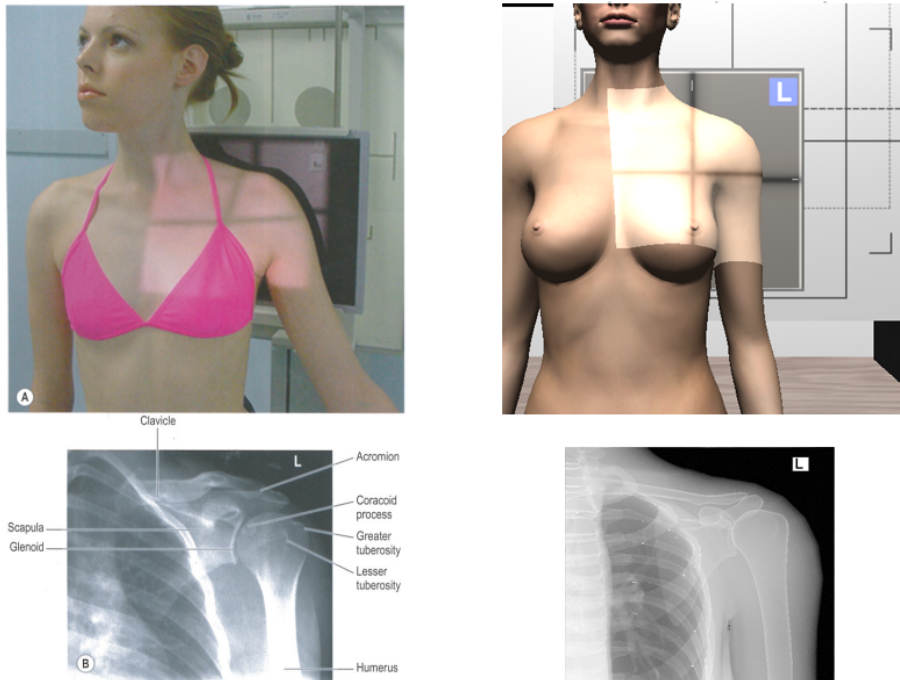
Figure 14: Likert scale responses of content validity.

---

Content validity	
C1:	Selecting the patient pose from a set of predefined ones is useful for self-guided training.
C2:	Selecting the patient manually is useful for self-guided training.
C3:	Selecting the patient pose from a set of predefined ones is useful to teach the procedure.
C4:	Selecting the patient manually is useful for teaching purposes (e.g. for live demonstration in the lecture theatre).
C5:	Regarding the previously described steps, the simulator is useful to teach the procedure.
C6:	Regarding the previously described steps, the simulator is useful for self-guided training.
C7:	In general, digital image manipulation of the X-ray image is useful for self-guided training and teaching.
C8:	Regarding the functionality described, this is useful to teach the procedure.
C9:	Regarding the functionality described, the simulator is useful for self-guided training.
C10:	Generally speaking, the simulator is suitable is useful as a teaching tool.
C11:	Generally speaking, the simulator is suitable for self-guided training.

---

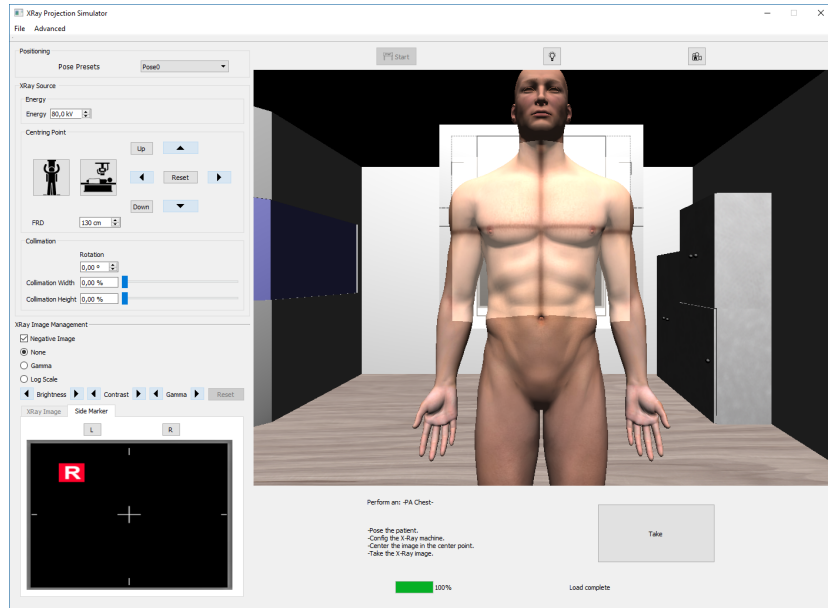
Table 3: Content validity statements



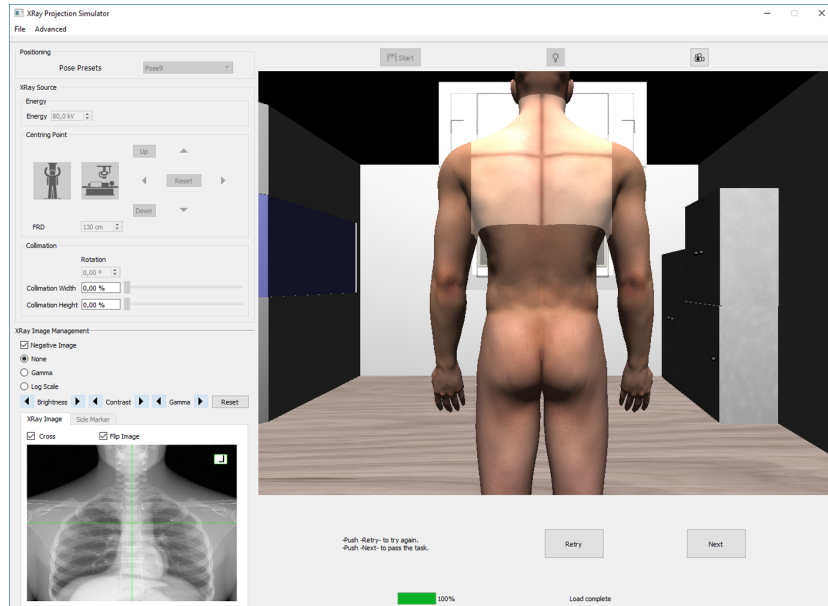
(a) Image courtesy of E. Carver, B. Carver and Elsevier Health Sciences [47].

(b) Projection replicated in the simulator.

Figure 15: Our system can replicate any type of projection, allowing the user to select the patient position and the X-ray configuration.



(a) Student must select a position without any hint and take a image without X-ray.



(b) Student can revise the result before next exercises.

Figure 16: GUI in non-guided training mode.